SANDIA REPORT
SAND2020-10723
Printed Sept 2020

Sandia National Laboratories

Diagnosing Field Strengths and Plasma Conditions in Magnetically Insulated Transmission Lines Using Active Dopant Spectroscopy

Sonal Patel, Brian Hutsel, Adam Steiner, Lawrence Perea, Deanna Jaramillo

Prepared by
Sandia National Laboratories
Albuquerque, New Mexico 87185
Livermore, California 94550

Issued by Sandia National Laboratories, operated for the United States Department of Energy by National Technology & Engineering Solutions of Sandia, LLC.

Available to DOE and DOE contractors from

U.S. Department of Energy
Office of Scientific and Technical Information
P.O. Box 62
Oak Ridge, TN 37831

Telephone: (865) 576-8401
Facsimile: (865) 576-5728
E-Mail: reports@osti.gov
Online ordering: http://www.osti.gov/scitech

Available to the public from

U.S. Department of Commerce
National Technical Information Service
5301 Shawnee Road
Alexandria, VA 22312

Telephone: (800) 553-6847
Facsimile: (703) 605-6900
E-Mail: orders@ntis.gov
Online order: https://classic.ntis.gov/help/order-methods

Diagnosing Field Strengths and Plasma Conditions in Magnetically Insulated Transmission Lines Using Active Dopant Spectroscopy

SAND2020-10723

ABSTRACT

Experimental validation data is needed to inform simulations of large pulsed power devices which are in development to understand and improve existing accelerators and inform future pulsed power capabilities. Using current spectroscopic techniques on the Z-machine, we have been unable to reliably diagnose plasma conditions and electric and magnetic fields within power flow regions.

Laser ablation of a material produces a low density plasma, resulting in narrow spectroscopic line widths. By introducing a laser ablated plasma to the anode cathode gap of the Mykonos accelerator, we can monitor how the line shapes change due the current pulse by comparing these line shapes to spectral measurements taken without power flow. In this report we show several examples of measurements conducted on Mykonos on various dopant materials. We also show a negligible effect on power flow due to the presence of the ablation plasma for a range of parameters.

This project was funded as an LDRD under project number 218467.

ACKNOWLEDGMENT

Thanks to Dan Scoglietti, who helped align and setup the Mykonos active dopant beamline. Thanks also to Robert Obregon who loaded this hardware for every shot, Sean Simpson for discussions on lasers, Mark Johnston for discussions on fiber arrays, George Laity for supporting this diagnostic, and Mike Cuneo for suggesting this diagnostic technique in the first place.

CONTENTS

LIST OF FIGURES

LIST OF TABLES

1. INTRODUCTION

Currently, passive dopant spectroscopy is used to try to monitor electron densities, and field strengths on the Z-machine. Passive dopants rely on the Z current pulse to heat the electrodes and ablate a dopant material into the anode cathode (AK) gap. So far, measurements have been limited to the electrode surfaces or near the electrode surfaces, resulting in line shapes that are Stark dominated due to the high electron densities that are present on the surfaces. Measurements closer to the center of the AK gap have not been successful, as the electron densities are too low for our systems to measure in these regions. As shown in Figure 1-1, emission lines from Li I using passive dopants are noisy, quickly merge into the continuum, and are significantly broadened due to high electron densities close to the surfaces.

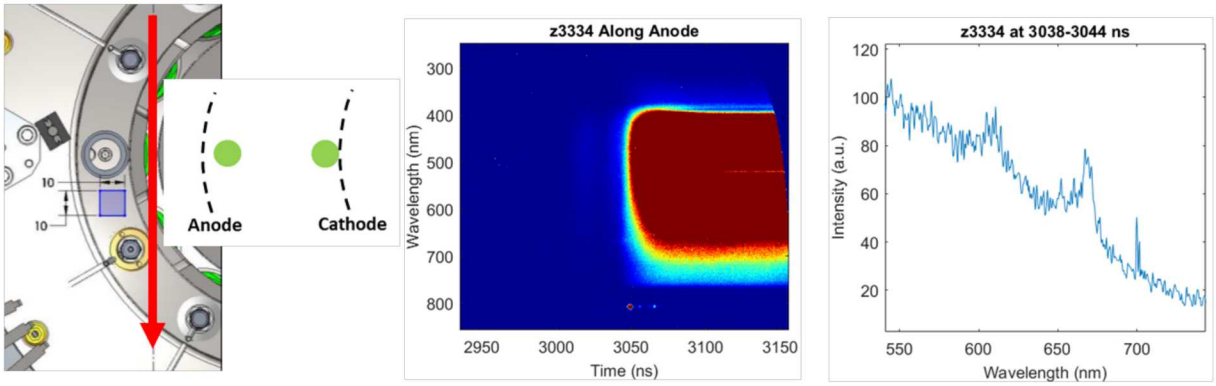

Figure 1-1 Measurements taken parallel to the anode and cathode on Z, in the axial extension (from M. Johnston) using streaked visible spectroscopy. The probe views along the red arrow. A lithium fluoride dopant was applied to the anode and cathode.

Viewing further off the electrode surfaces and into the AK gap, spectroscopic measurements can be improved to enable estimates of relevant parameters such as plasma densities, temperatures, magnetic and electric fields. Such measurements are crucial to verifying models for the Z-machine and future capabilities. It would also provide new optical diagnostic capabilities for plasma parameters in regions where passive dopant spectroscopy cannot probe.

However, to accomplish this the signal intensity must be improved. One way to improve line intensities is to use active dopant spectroscopy. Experiments conducted during an Exploratory Express LDRD suggest that electron densities less than 1×10^{16}–5×10^{16} cm^{-3} can be produced and measured using a laser to ablate material from a stainless steel, doped surface. As shown in Figure 1-2, this results in narrow line widths which can be used to monitor changes in the line shape due to the power pulse. Comparing Figure 1-2 to Figure 1-1, the laser ablation plume provides clean spectral emission lines from a lower density plasma. With sufficient spectral resolution changes in these line shapes due to perturbations not related to the initial ablation plasma can be used to infer electric, magnetic fields and electron densities. This technique can also provide spatially resolved measurements across the AK gap, as the ablation plasma extends a few millimeters from the target surface.

This diagnostic was implemented on the Mykonos accelerator [1] in order to determine the effect the ablation plasma may have on power flow. Mykonos produces about a 1 MA, 500 kV pulse

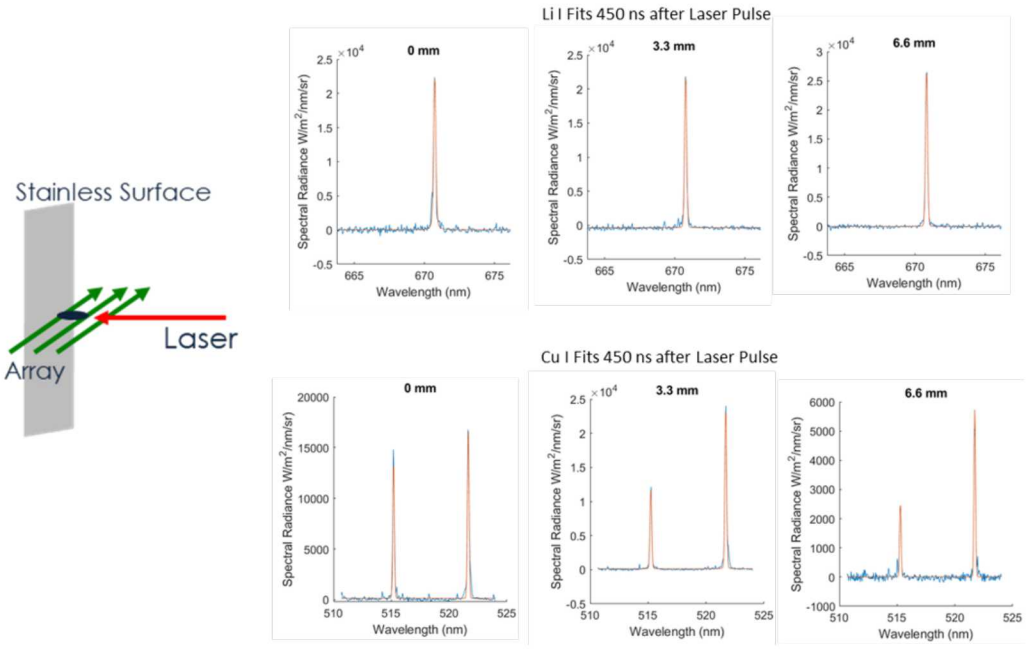

Figure 1-2 Measurements taken parallel to the ablation target surface using a 7-fiber array. The line widths are at the instrument resolution and suggest electron densities less than $4 \times 10^{16}\,\mathrm{cm}^{-3}$ from Li I, and less than $1 \times 10^{16}\,\mathrm{cm}^{-3}$ from Cu I. A LiF coating was applied to a 304 stainless surface for the Li I measurements, and a pure copper sheet was used for the Cu I fits. A 3 ns gate time was used for these data.

into a 0.5 Ω matched load. In this report, we show that we can produce an ablation plasma that has a negligible effect on current delivery. We measure line emission from several dopant materials during the Mykonos power pulse and estimate electron densities and temperatures form these various materials.

2. EXPERIMENTAL SETUP

As shown in Figur 2-1 the load hardware consist of a coaxial transmission line which transitions to radial transmission line. An inductive cavity in the cathode is used to increase the electric field stress at the dopant plug. A 0.25 in solid stainless rod is used to bridge the AK gap. The laser is introduced 4 cm off axis onto a removable dopant plug. Various plug materials were fielded including solid copper and aluminum plugs, and LiF and NaCl coatings on stainless steel plugs to mimic potential fielding options on Z. 4 A-level B-dots are fielded upstream of the ablation plasma, and the 4 load B-dots are fielded downstream of this plasma. By comparing current estimates between these B-dots we can estimate the amount of current that may be shunted through the ablation channel. Figure 2-1b shows a close up of the Mykonos hardware. A 90 degree turning mirror is used to steer the beam to the dopant plug through a minimum 3 mm hole at the anode.

The AK gap is adjustable up to 10 mm using shims placed between the anode and return can. The majority of our measurements were fielded at a 4.5 mm gap. However, to prevent gap closure for

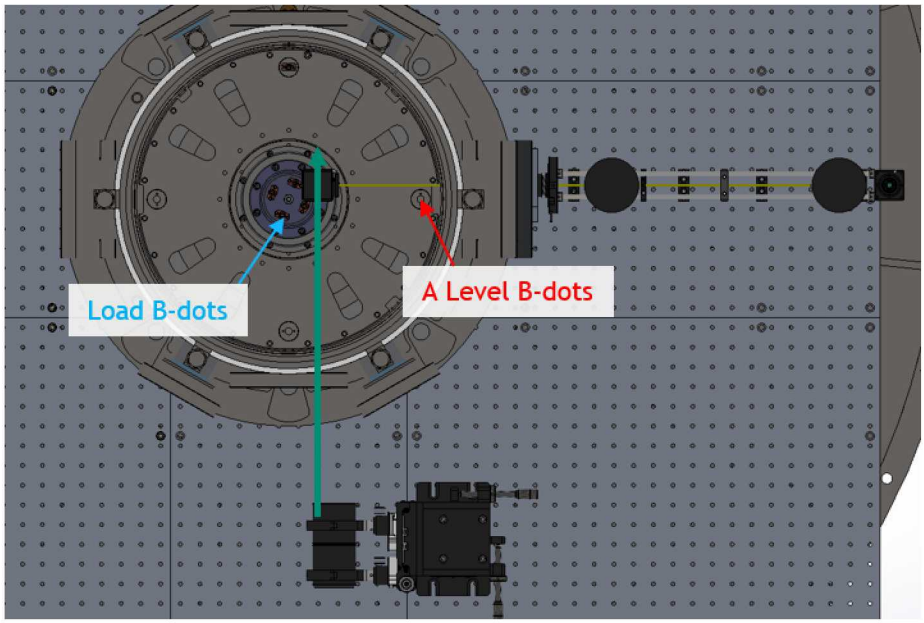

(a) Mykonos Chamber

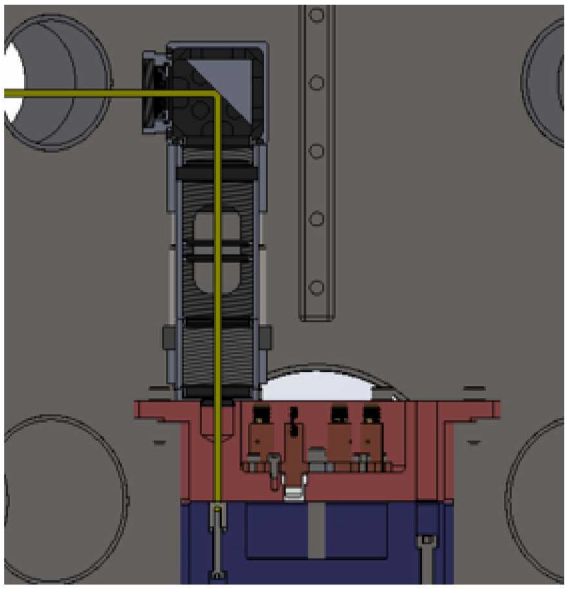

(b) Load Hardware

Figure 2-1 Mykonos Load Hardware. The yellow lines represent the laser beamline, and the green arrow represents the spectroscopy line of sight. B-dots are fielded upstream (A level) and downstream of the ablation plasma (Load)

some configurations many of the measurements were fielded at over 6 mm gaps. These details are explained further in Section 3. The geometry is shown in more detail in Figure 2-2. Figure 2-3 shows the 3 mm hole that introduces the laser plasma adjusts the electric field slightly. In the case of a 3 mm gap, the field changes from about 0.62 MV/cm to 0.5-0.55 MV/cm.

The 0.25 in solid stainless rod did not need to be replaced every shot. As a result, we were able to repetitively shoot Mykonos without breaking vacuum and reloading between every shot. We only reloaded if the vacuum insulator flashed and required refurbishment or if the AK gap shorted due to the laser plasma. In this case the focusing lens became coated and/or damaged and needed to be replaced. Deposition would also occur on the anode and cathode around the dopant plug which needed to be sanded.

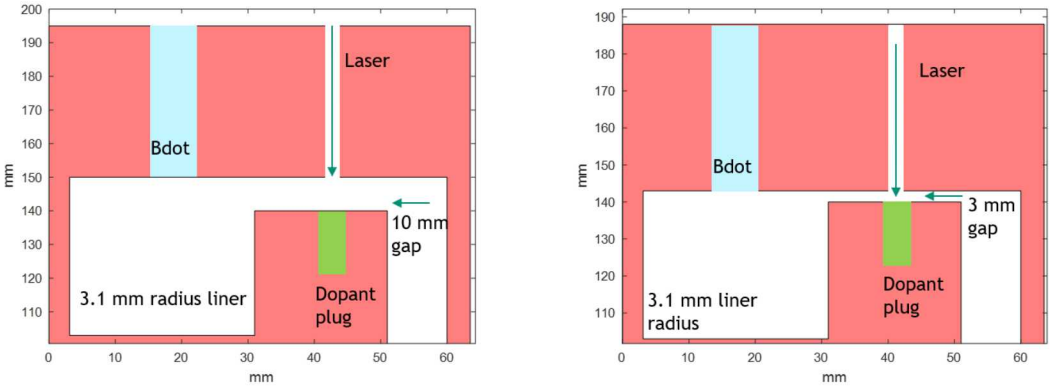

(a) 10 mm Gap, 22 nH, 0.22 MV/cm **(b) 3 mm Gap, 18.7 nH, 0.62 MV/cm**

Figure 2-2 Hardware Geometry

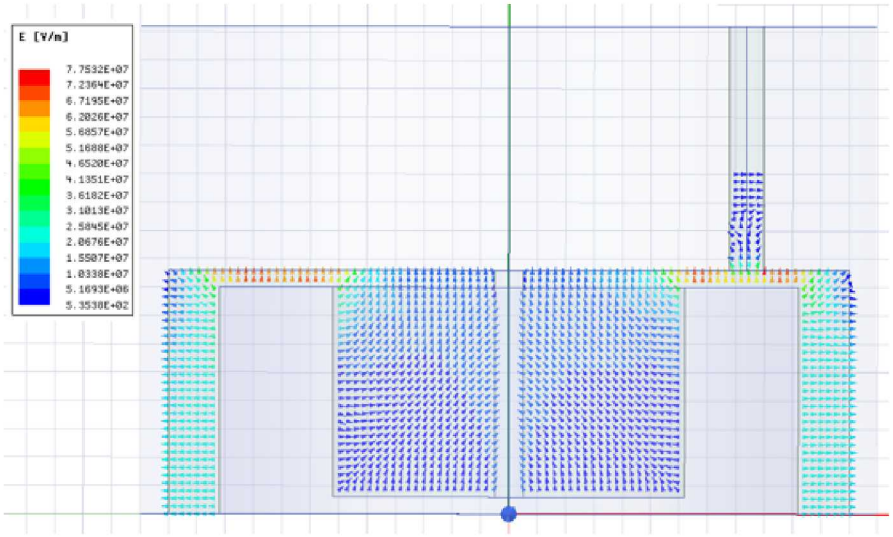

Figure 2-3 Maxwell simulation of a 3mm Gap and 3mm laser entrance hole.

A Continuum Surelite Ex 1064 nm, Nd:YAG, 700 mJ laser is used to ablate material that is measured spectroscopically. Although the laser can reach 700 mJ, it was fielded at energies less than 110 mJ (with one shot at 200 mJ) at the laser output. Approximately only half the laser

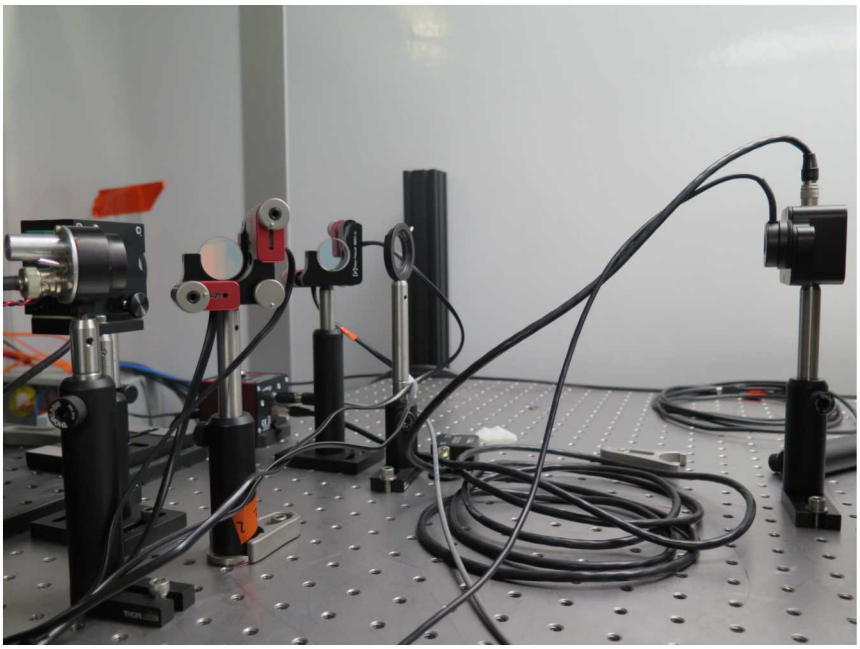

(a) Entrance to the Mykonos beamline

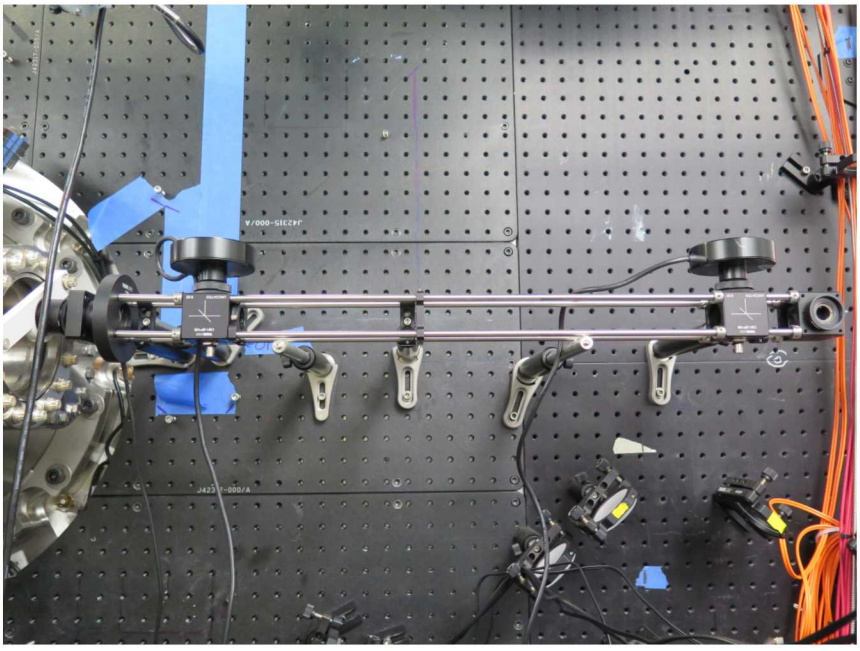

(b) Mykonos beamline

Figure 2-4 Ablation laser setup

energy reaches the target due to losses in the beamline and at the vacuum window. The majority of the shots here were fielded with laser energies of 45-50 mJ at the target. Figure 2-4 shows the entrance to the Mykonos beamline (a) and the beamline that enters the vacuum chamber (b).

The approximately 9.5 mm beam exits the laser and passes through an external variable attenuator which consists of a 1/2 waveplate and plate polarizer. A portion of the discarded beam is

measured with a photodiode, which provides timing information. Two turning mirrors steer the beam remotely into the Mykonos beamline. Within the beamline shown in 2-4, two pellicle beam splitters pick off a few percent of the beam energy at 90 degrees which is relayed to an energy meter and quad diode sensor, as shown in Figure 2-4. The quad diode comprises the position sensing detector, allowing for remote alignment of the beam to the the optical axis and experiment. The beam is aligned to the center of the quad diode (positioned at 90 degrees to the optical axis). A remote shutter, just before the vacuum chamber window, is used to align the beam without ablating the target material. Once alignments are completed, the laser is switched to single shot mode, and the shutter is opened. The beam passes into a vacuum chamber where a 100 mm focal length lens focuses the beam onto the target, resulting in a calculated focused beam size of 0.1 mm.

A double fiber array images the ablation plasma and is coupled to a 2/3 m Mcpherson spectrometer. A sketch and beam profile of the array is shown in Figure 2-5. Each fiber in the array is focused to about 0.5 mm at the ablation plasma. One column is aligned to the ablation plasma axis, found by linearly moving the array to the highest intensity plasma. The second column measured off axis from the brightest plasma region. There are two advantages to this approach. Off axis measurements are at lower plasma densities and are therefore more sensitive to changes in plasma density and/or field strengths due to the Mykonos power pulse. In cases were we used a 0.5 μm coating on a stainless steel plug for the dopant, detailed alignments, in which we move the array until it matches the ablation plume axis were not possible without ablating the dopant prior to the shot. The double fiber array decreases the precision needed for alignments.For this reason a double or even triple fiber array will likely be used on the Z-Machine in future iterations of this diagnostic.

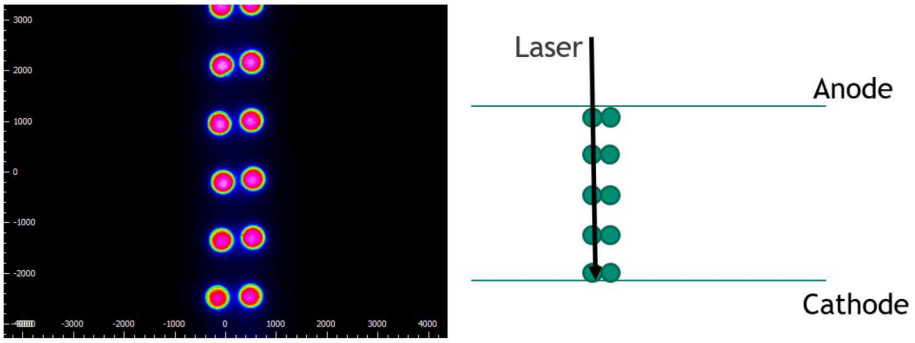

(a) Beam profile of the fiber array. **(b) Sketch of the array.**

Figure 2-5 Double fiber array that is used to image the AK gap and ablation plume. The array is focused to about 0.5 mm regions at the laser plasma and one column is aligned to the axis of the laser plasma.

The spectrometer is typically gated for 10 ns with a gain of 80. The resolution depends on the grating used and the slit size. Aside from measurements of the copper plasma we used a 1200 g/mm grating with a resolution of 0.12-0.14 nm. For copper dopants we used a 600 g/mm grating in order to capture Cu II and Cu III lines in addition to Cu I for estimates of electron temperatures, these measurements had resolutions of 0.3 nm.

3. EXPERIMENTAL RESULTS

A total of 60 shots were fielded. These are summarized in Appendix A. For every shot measuring the laser ablation a preshot or post shot was taken to monitor the spectral line shapes without power flow. These spectra can be compared to the shot spectra, and changes in the line shapes can be attributed to the current pulse. For consumable dopant plugs in which a thin film coating (LiF or NaCl) was applied, post shot spectra were taken in the same location as the shot spectra. Although less material is present during the post shot spectra for consumable dopants, there is still enough material that certain parameters such as electron densities could be compared. In order to obtain multiple shots without breaking vacuum and replacing these dopant plugs, the laser was moved slightly along the line of sight of the fiber array between shots (About 0.1mm). We achieved up to about 3 shots using this method before the AK gap entrance partially cut off the laser. In this section we show some representative analysis of these shots.

3.1. B-dot Calibrations

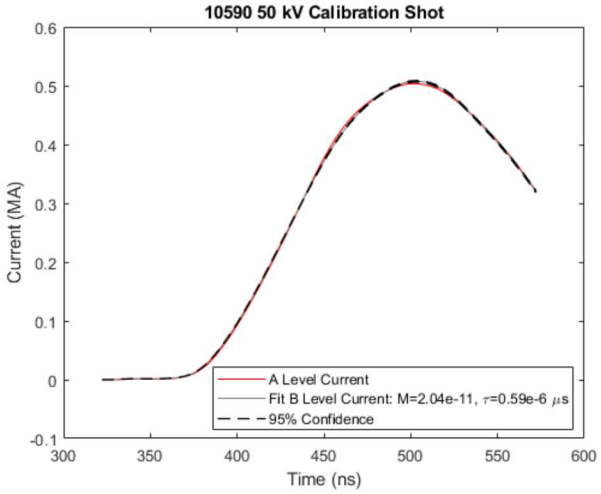

Figure 3-1 50 kV Calibration shot and fit for M and τ_f

Figure 2-1a shows the locations of the B-dots. In order to determine whether power flow is adversely affected by the presence of the ablation plasma, the load B-dots are compared primarily to null shots in which the laser plasma is not present, but they are also compared to the A-level current measurement on every shot. A shot at 50 kV was used to calibrate the load B-dots against the A-level B-dots using Equation 1, from [2]. τ_f is also a fit parameter in this model and is used to account for differences in flux-penetration times.

$$I = \frac{\exp(-\frac{t}{\tau_f})}{M} \int_0^t V \exp(\frac{t}{\tau_f}) dt \tag{1}$$

Since null shots were taken only at every gap size, and not each time the hardware was reloaded, small changes in the B-dot positioning may affect these M and τ_f values resulting in small offsets

in the current (<5%) between the null shots and laser ablation shots. Additionally, jitter in the Mykonos switch timing and trigger circuit can also lead to small differences in peak current. Occasionally there was 10's of nanoseconds of jitter in the Mykonos trigger, in this case the null shots were lined up at 10% of peak current to more easily compare potential current loss.

Figure 3-1 shows the results of the 50 kV calibration shots, assuming no loss at 50 kV. The τ_f and M values shown in Figure 3-1 are used for all of the active dopant shots so far on Mykonos.

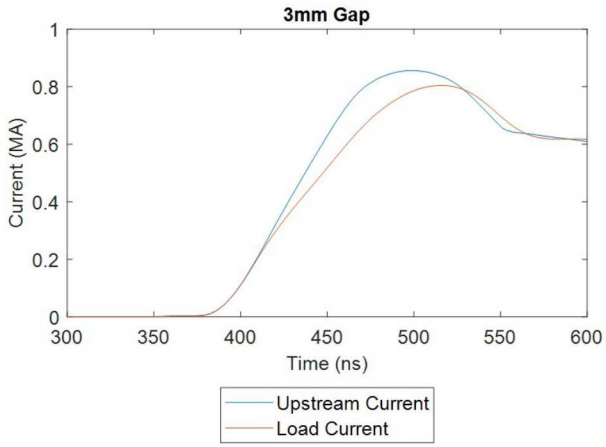

(a)

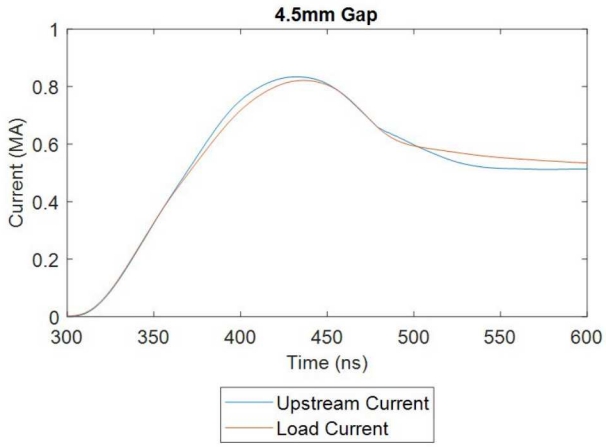

(b)

Figure 3-2 Current loss due to gap size.

The majority of these shots were taken at an AK gap size of 4.5 mm because at 3 mm there appeared to be significant loss, even without the presence of the ablation plasma. This is shown in Figure 3-2. The majority of the 4.5 mm shots showed similar levels of loss as in 3-2b, with the exception of shots between 10645-10650. This set showed higher loss at the 4.5 mm gap than was typical. A null shot (without the ablation plasma) was taken prior to removing and refurbishing the hardware in this set. The null shot and shots with an ablation plasma showed very similar levels of loss, which suggests that the hardware was responsible for most of this loss, and not the laser plasma. Current traces from two shots in this set are shown in Figure 3-5.

3.2. Copper

Copper has several strong Cu I, II, III spectral lines between 500-530 nm. Relatively high resolution measurements can be made in this region to obtain estimates of line broadening and temperature from Cu line ratios of various ionization states. A resolution of 0.3 nm was used for measurements of the copper plasma. We used a solid copper plug for the ablation target.

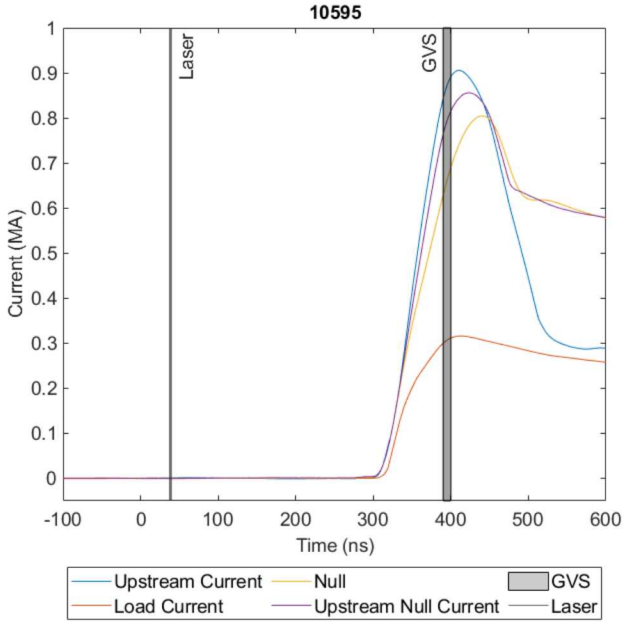

Figure 3-3 80 kV shot, 100 mJ laser energy, laser triggered 368 ns before peak current.

In order to obtain consistent and narrow line widths so that the line shapes are not Stark dominated due to the ablation plasma itself, we determined from light lab experiments that it is best to trigger the laser several 100 nanoseconds before the required measurements. Figure 1-2 shows an example of this, where the laser is triggered 450 ns prior to the spectra. However, at several hundred nanoseconds prior to the Mykonos current pulse, we found that the laser expands into the gap with sufficient density that it can shunt more than half the current through the ablation channel. When this happens the spectra is often completely saturated, suggesting very hot, dense plasma. Figure 3-3 shows current traces from a shot that had a 3 mm gap, 100 mJ laser energy at the ablation target (same laser energy as Figure 1-2), and a laser trigger about 368 ns before peak current.

Even when we lowered the laser energy considerably, we measure lower current than expected. Figure 3-4 shows a shot with a 4.5 mm gap, 15 mJ laser energy, and a laser trigger about 317 ns before peak current. For reference, all the copper dopant shots (except those with extreme shorting where over half the current is lost in the laser plasma) had currents between 0.81-0.82 MA.

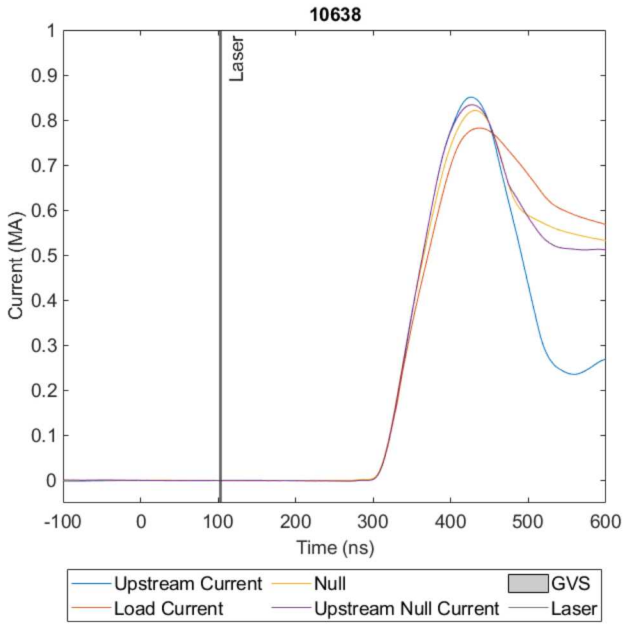

Figure 3-4 80 kV shot, 15 mJ laser energy, laser triggered 368 ns before peak current.

3.2.1. Shot 10648 and 10645

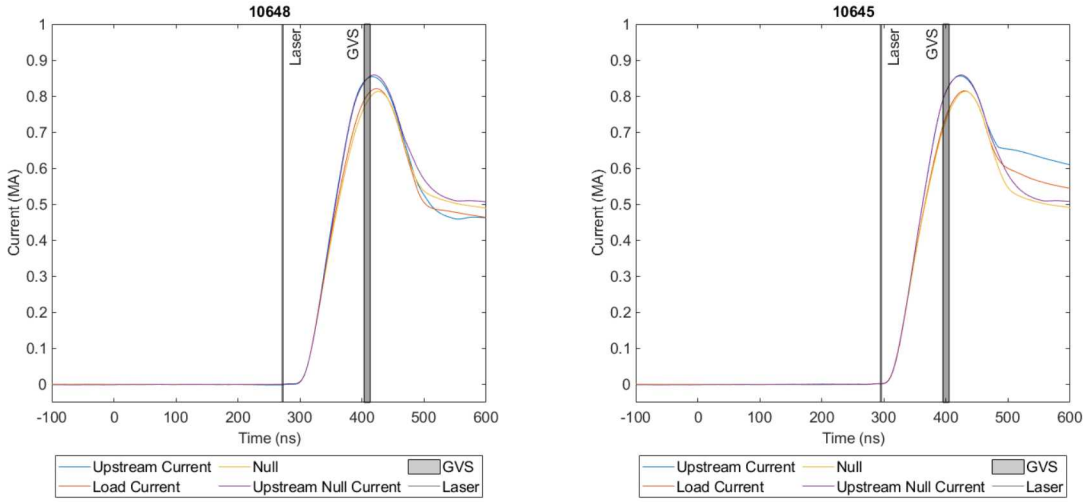

(a) 51 mJ **(b) 30 mJ**

Figure 3-5 Current traces for two copper dopant shots with differing laser energies.

Shot 10648 is analyzed here in more detail. This shot has a 51 mJ laser energy at the ablation target, a peak current of 0.82 MA, a 4.5 mm AK gap, and a spectral resolution of 0.3 nm. Current traces are shown in Figure 3-5. As discussed in Section 3.2 this set of copper shots has more loss

for the null the ablation plasma cases, which suggests that the loss is due to this hardware configuration or setup, rather than the laser plasma. The null shot has similar currents (within 2%) of the ablation shots.

Preshot and shot spectra are shown in Figure 3-6. The preshot spectra contains Cu I line emission along the cathode surface, with Cu II lines about 1 mm from the surface. In contrast, the shot spectra contains Cu III and Cu II lines 1 mm from the surface, indicating a higher temperature plasma caused by the Mykonos power pulse.

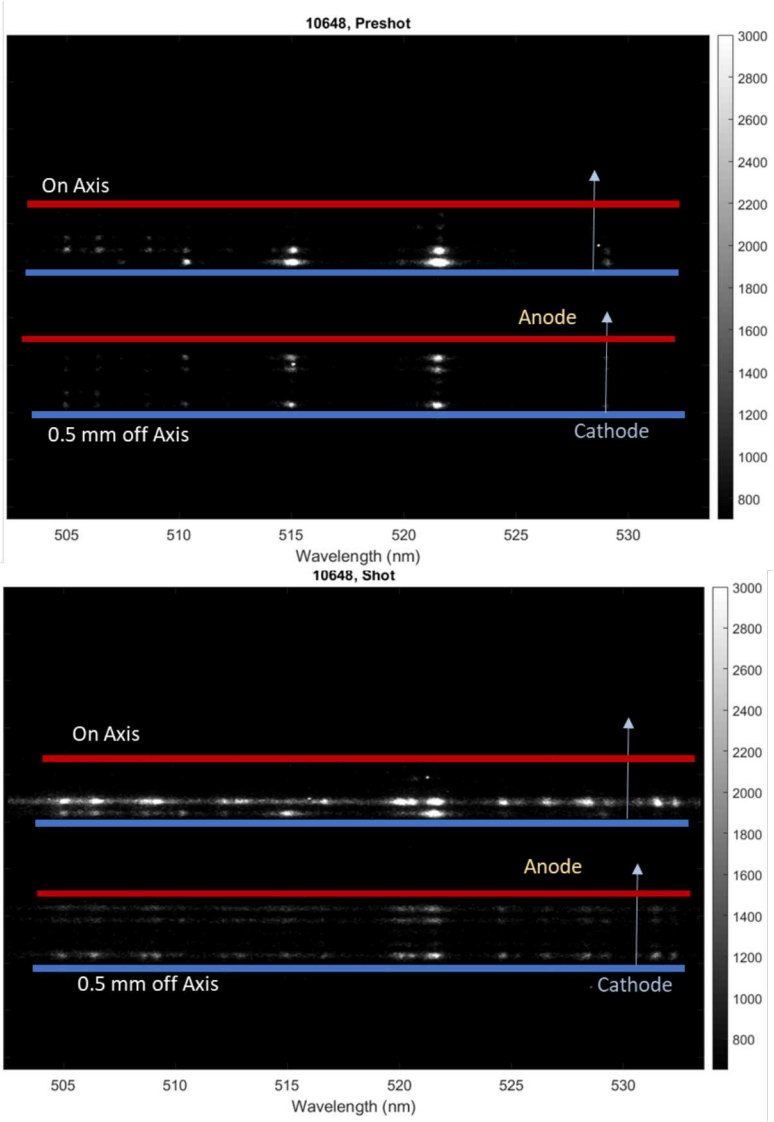

Figure 3-6 Shot 10648 preshot and shot spectra.

Due to divergences in the LTE and nLTE line ratio calculations in PrismSPECT, plotted in Figure 3-7, PrismSPECT [3] was used to calculate nLTE Cu I/Cu II and Cu II/Cu III line ratios to obtain electron temperatures. A plasma length of 1.5 mm was assumed along the spectral line of sight (the extent of the fiber array, outside of which ion densities are likely much lower than the on axis plasma). However, this was not directly measured, and even at this length, opacity effects for Cu I

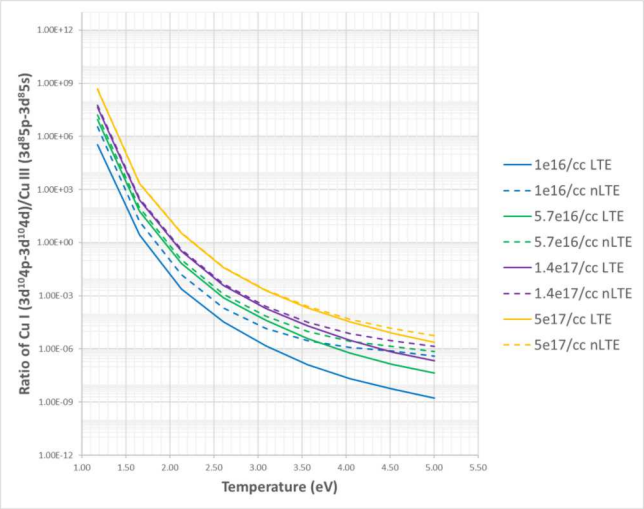

Figure 3-7 Cu I/CuIII line ratio in LTE and nLTE.

should be more carefully considered. In the case of a larger optical depth, the Cu I/Cu II ratio would be higher than shown here, and we would underestimate the temperature. However, temperatures for the preshot plasma are likely less than 2 eV, (since by about 2 eV the Cu II/Cu III line ratio should be about 1. Figure 3-8 shows the spectral lines used and the line ratios to obtain electron temperatures.

Electron densities were estimated by fitting only the Cu I lines with sufficient signal to noise ($3d^{10}4p - 3d^{10}4d$ and $3d^{9}4s2 - 3d^{10}4p$) using stark widths from [4]. Therefore, electron densities were not estimated in the middle of the gap due to insufficient Cu I signals in that region. From Figure 3-6 the intensity of Cu I and Cu III drops towards the middle of the gap. It's possible that the temperature continues to increase into the gap where densities are lower, and the neutral and C III ion concentration is much lower in this region. The temperature may lower at the anode as the plasma interacts with the electrode surface. The off axis plasma is at higher temperatures likely due to the lower electron densities in this region. An example fit of the Cu I lines is shown in Figure 3-9 and a summary of electron temperatures and densities for the preshot and shot spectra is in Table 3-1.

Table 3-1 Summary of Shot 10648 temperature and density changes

Axis (mm)	Preshot Density (cm-3)	Shot Density (cm-3)	Preshot T (eV)	Shot T (eV)	ΔDensity (cm-3)	ΔT (eV)
0	9.80E+16	1.50E+17		1.3	5.20E+16	
1	5.10E+16		1.3	2.6		1.3
2			1.5			
3						
4						
Off Axis (mm)	Preshot Density (cm-3)	Shot Density (cm-3)	Preshot T (eV)	Shot T (eV)	ΔDensity (cm-3)	ΔT (eV)
0	5.60E+16	1.50E+17	1.25	2.7	9.40E+16	1.45
1						
2						
3	8.90E+16		1.3	2.75		1.45
4	7.00E+16		1.2	2.7	1.5	1.5

It is still unclear why the temperature increases by about 1.3-1.5 eV within about 1 mm of the anode and cathode during the shot, when compared to the preshot. One explanation is that we

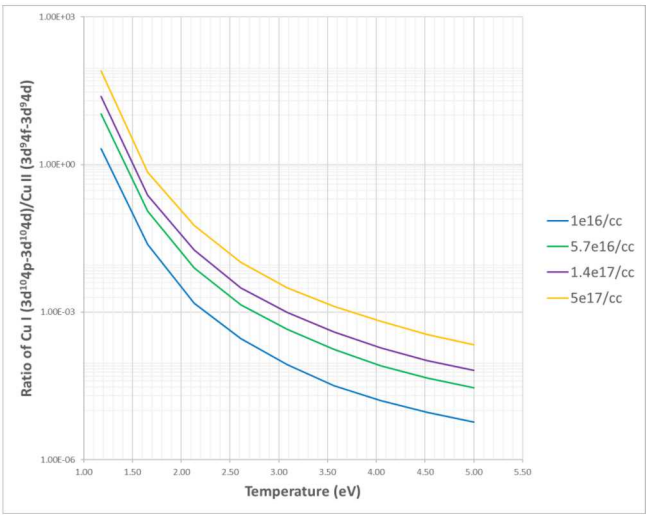

(a) CuI/CuII

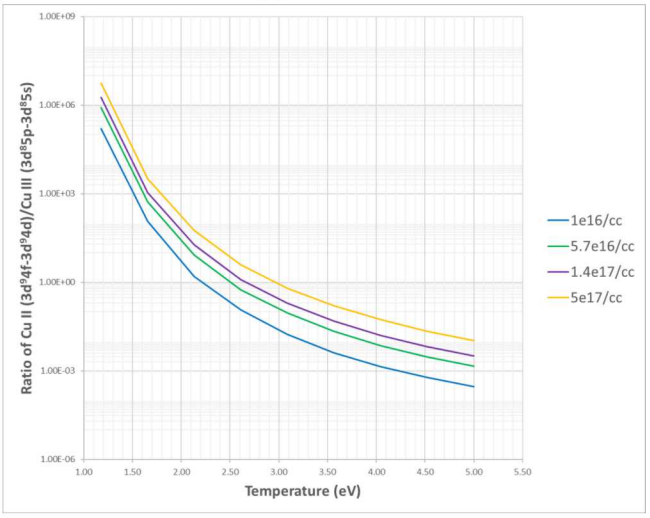

(b) CuII/CuIII

Figure 3-8 PrismSPECT line ratios for the relevant emission lines used to estimate electron temperatures.

current is shunting through this channel within the uncertainty of the B-dot estimates. However, the majority of our measurements on this dopant and gap size are all within 1% of each other and the null (with the exception of more obvious shorting). Furthermore, in [5] the authors use a 20 J, 1054 nm, 0.1 mm focused diameter laser (resulting in nearly 500 times the energy density of the Mykonos laser system) in order to create the conducting load for the Zebra accelerator. They measure a temperature increase of about 0.8 eV with about 200 kA through the ablation channel. In contrast, on Shot 10648 we measure an average temperature increase of 1.4 eV with likely not more than 20-30 kA through this channel.

The effect of varying laser energies were also studied using copper dopants. Figure 3-5 shows current traces using laser energies of 51 mJ and 30 mJ. Figure 3-10 compares spectra along the cathode surface for these laser energies. Line intensities are reduced significantly by reducing the

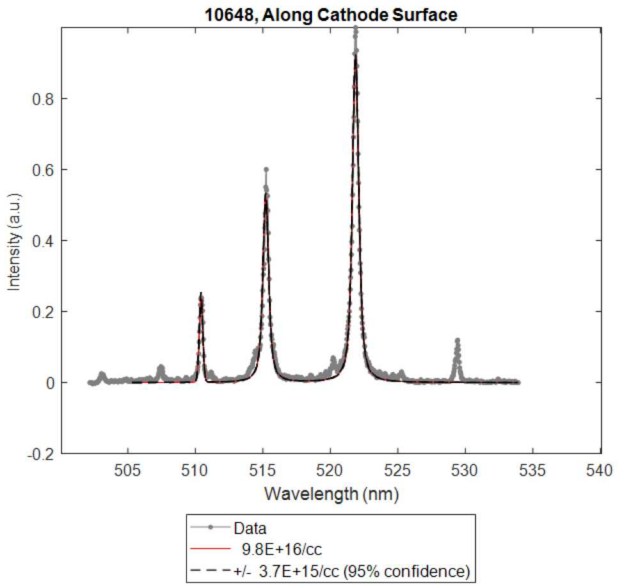

Figure 3-9 Example preshot spectral profile fit of Cu I lines for the on axis ablation plasma.

laser energy, even though the load current remains nearly the same. As a result, the majority of the active dopant shots on Mykonos were taken using laser energies between 45-55 mJ.

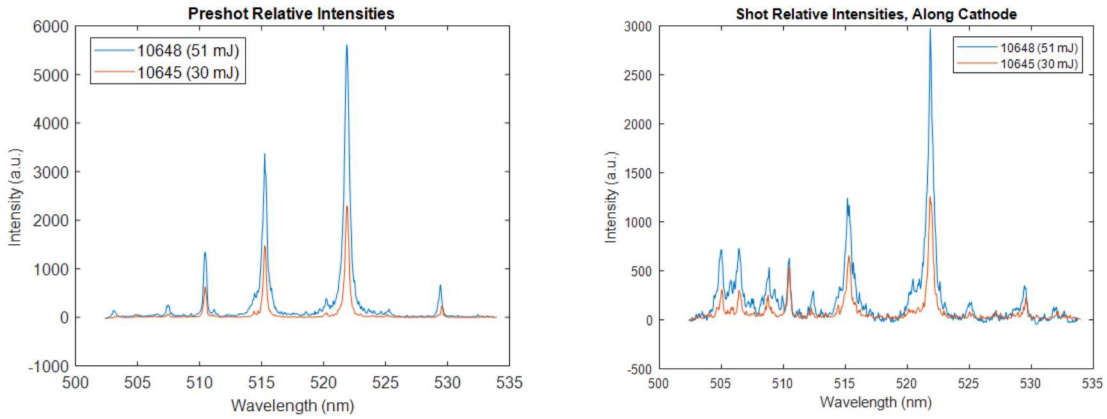

(a) CuI/CuII **(b) CuII/CuIII**

Figure 3-10 Comparison of spectral line intensity using laser energies of 51 mJ and 30 mJ.

3.3. Aluminum

Aluminum is also used as a dopant for this active dopant diagnostic. Specifically, the $3s^2 3p - 3s^2 4s$ doublet at 394.4 and 396.2 nm was measured spectroscopically with a resolution of 0.12 nm using a 1200 g/mm grating. This line is well isolated and can potentially be used for

magnetic field measurements. Even in the case of Stark dominated line shapes from the laser ablation plasmas shown here, the magnetic field can potentially be determined using relative widths between the doublet line as discussed in [6]. Here we assume only density broadening, more detailed line shape analysis is still likely required. In the case of fields distorting the line shapes, the density estimates shown would be too high.

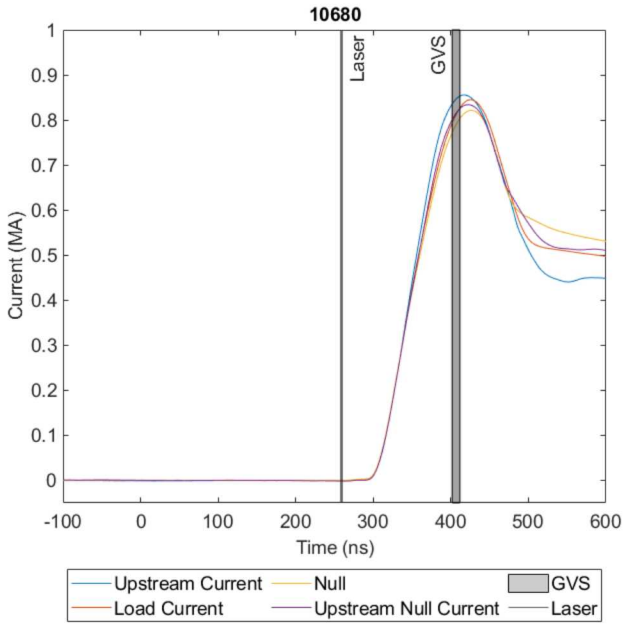

Figure 3-11 Shot 10680, Aluminum dopant, 4.5 mm Gap, 45 mJ laser energy, 0.14 nm spectral resolution.

Figure 3-11 shows current traces from an example shot with an aluminum dopant. In this case the laser was triggered about 150 ns prior to peak current and no loss was measured. Both the A-level B-dots and load B-dots measured slightly higher current than the null, but the current loss appears to be very similar between the two cases. The load current deviation from the upstream B-dots also occurs at similar times. For this reason we assume that no loss occured due to the ablation plasma. Spectra from this shot is shown in Figure 3-12.

The preshot spectra shows relatively strong emission lines across the gap, with broad emission lines along the cathode viewing through the axis of the ablation plasma. In the case of magnetic insulation during the shot we would expect increasing densities toward the electrode surfaces, but decreasing densities into the gap during the Mykonos shot.

This data also shows the importance of off axis measurements. When one column of the fiber array is aligned to the on axis plasma the second column measures significantly less broadened line emission. This is important for measurements of magnetic and electric fields which can be obscured by Stark broadening. The off axis measurements can provide relatively narrow line shapes without triggering the laser earlier which would likely cause the gap to short.

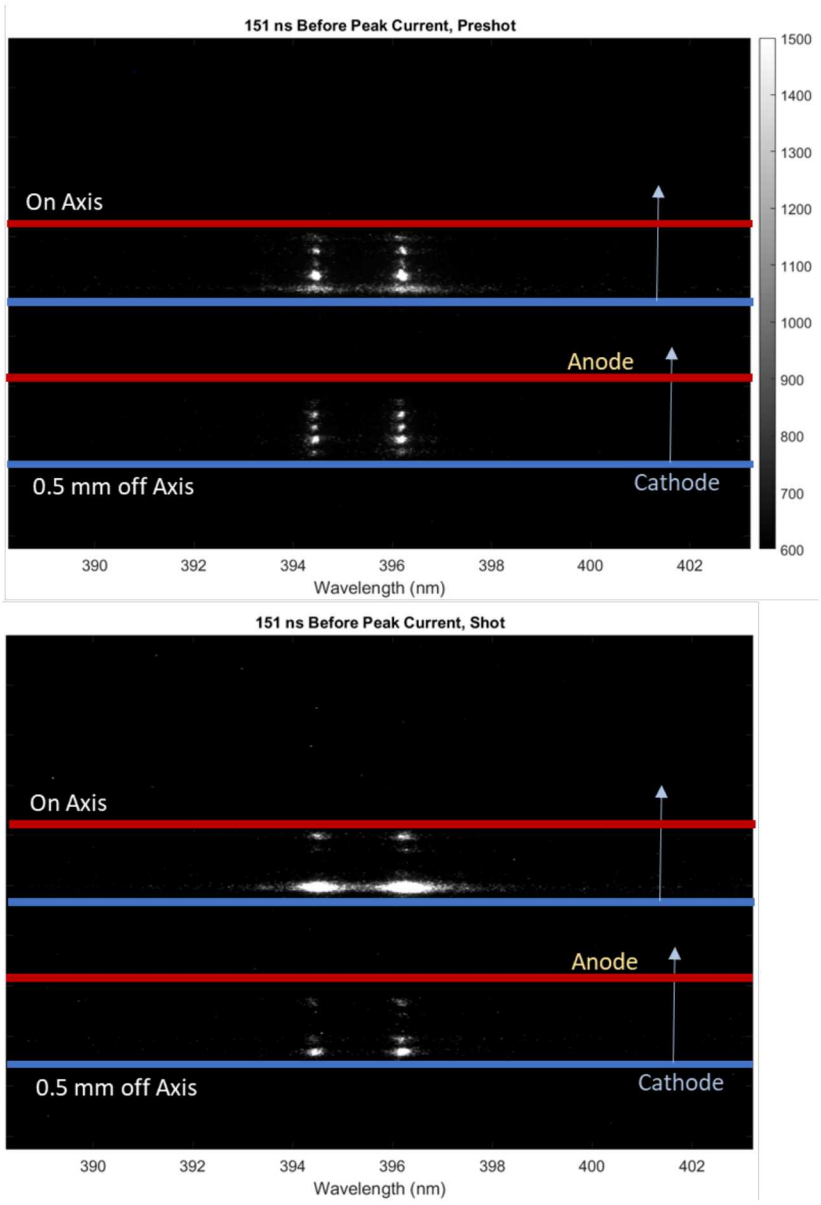

Figure 3-12 Shot 10680 spectra.

Figure 3-13a shows off axis density estimates from several shots as a function of laser time within 1 mm of the cathode. And Figure 3-13b shows the change in density between the shot and preshot as a function laser time for on axis and off axis spectra. Example fits are in Figure 3-14. Stark widths are from [4].

The on axis electron density appears to decrease between the preshot and shot spectra for most of these shots, while the off axis, and 1 mm from the cathode densities increase. In the less stark dominated case of the off axis plasma (Figure 3-13a) the difference in electron density between the surface measurement and 1 mm from the cathode during the shot is much less than in the preshot spectra which suggests the electron density gradient is smaller during the shot then during the preshot which could potentially be a result of magnetic insulation. More than about 1 mm

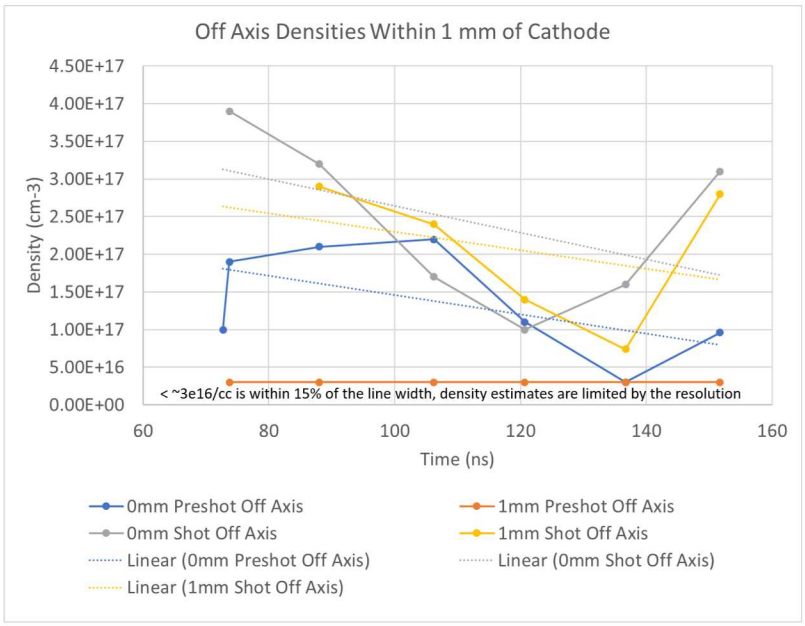

(a) Al Off Axis Density

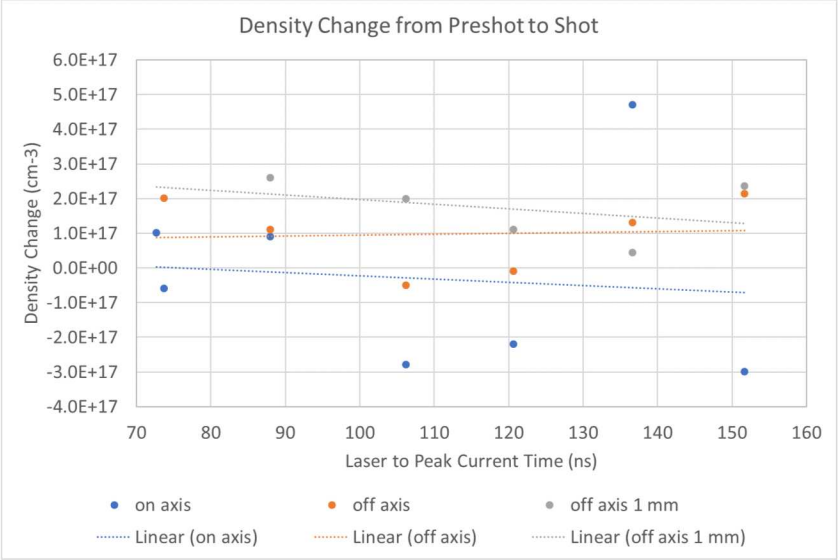

(b) Al Density Change

Figure 3-13 Electron density comparisons for Al dopants over 7 separate shots. All shots here used 45 mJ laser energy with 0.14 nm spectral resolution. No loss was measured on any of these shots.

from, the cathode the intensity drops during the shot towards the middle of the AK gap. Here the SNR is too low to accurately fit the line shapes. We expect higher temperatures in the middle of the gap. At these higher temperatures the neutral Al lines may drop in intensity. Additionally, we expect the electron density to decrease with increasing temperature. Furthermore, along the anode surface, the neutral Al lines are visible again during the shot, with higher electron densities then during the preshot (Figure 3-14), perhaps suggesting magnetic insulation. However, shot to shot spectral variation can be large, and uncertainties still need to be estimated. It may also be possible

that on some shots current is shunted, within the margin of error for the B-dots (we expect this is less than 20-30 kA), through the ablation plasma channel resulting in higher densities. Simulations could potentially provide more insight into temperature and density increases due to a few 10's of kA through a plasma channel.

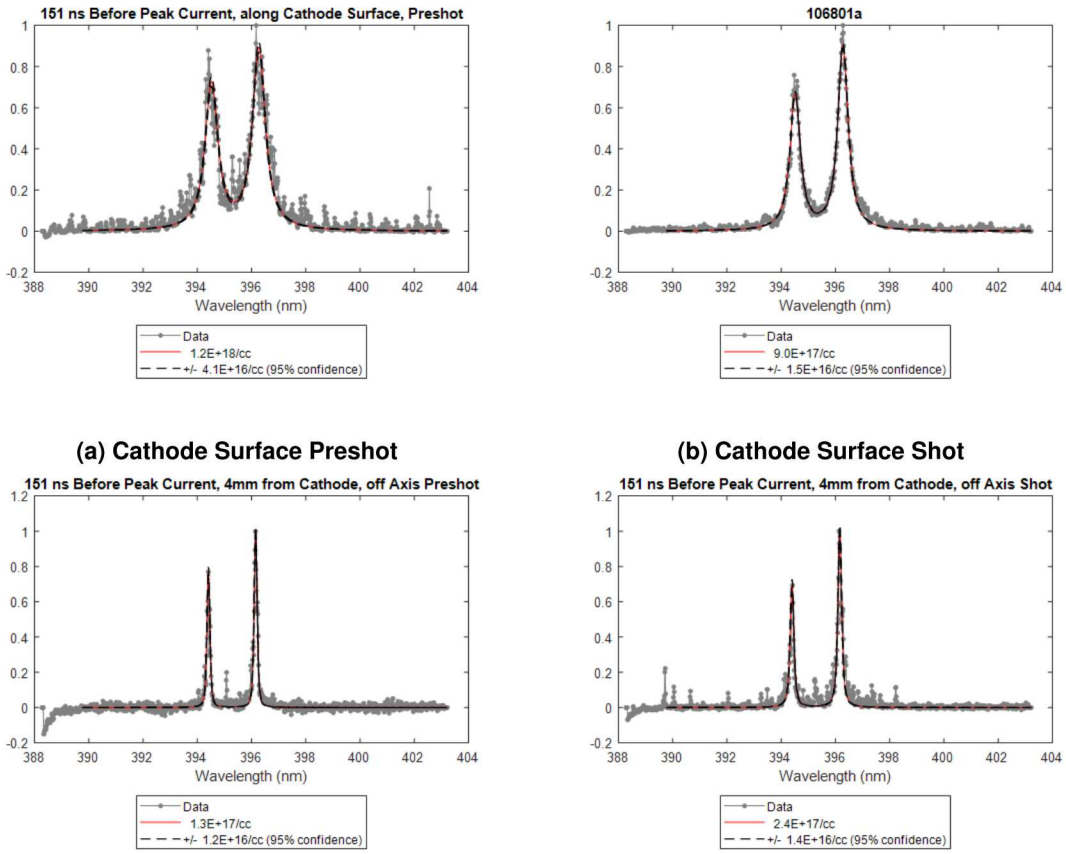

(a) Cathode Surface Preshot **(b) Cathode Surface Shot**

(c) Anode Surface Preshot **(d) Anode Surface Shot**

Figure 3-14 On axis electron density fits of Al I lines from shot 10680. Anode surface electron density increases by about 1e17/cc from the preshot, while cathode density decreases by about 3e17/cc

3.4. Sodium

A NaCl 0.5 um thin film coating over a stainless steel plug is also used to mimic passive dopant conditions on Z. Additionally the sodium D-lines have been used on Z to estimate magnetic fields from the Paschen-Back effect [7]. The majority of the B-dot traces from NaCl active dopant shots on Mykonos do not suggest current loss, however in this section we will show two borderline cases. Shot 10703 deviated more significantly from the A-level B-dots then normal, although peak current was typical. And shot 10695 had about 80 kA of loss. Figure 3-16 gives current traces from a typical shot 10690.

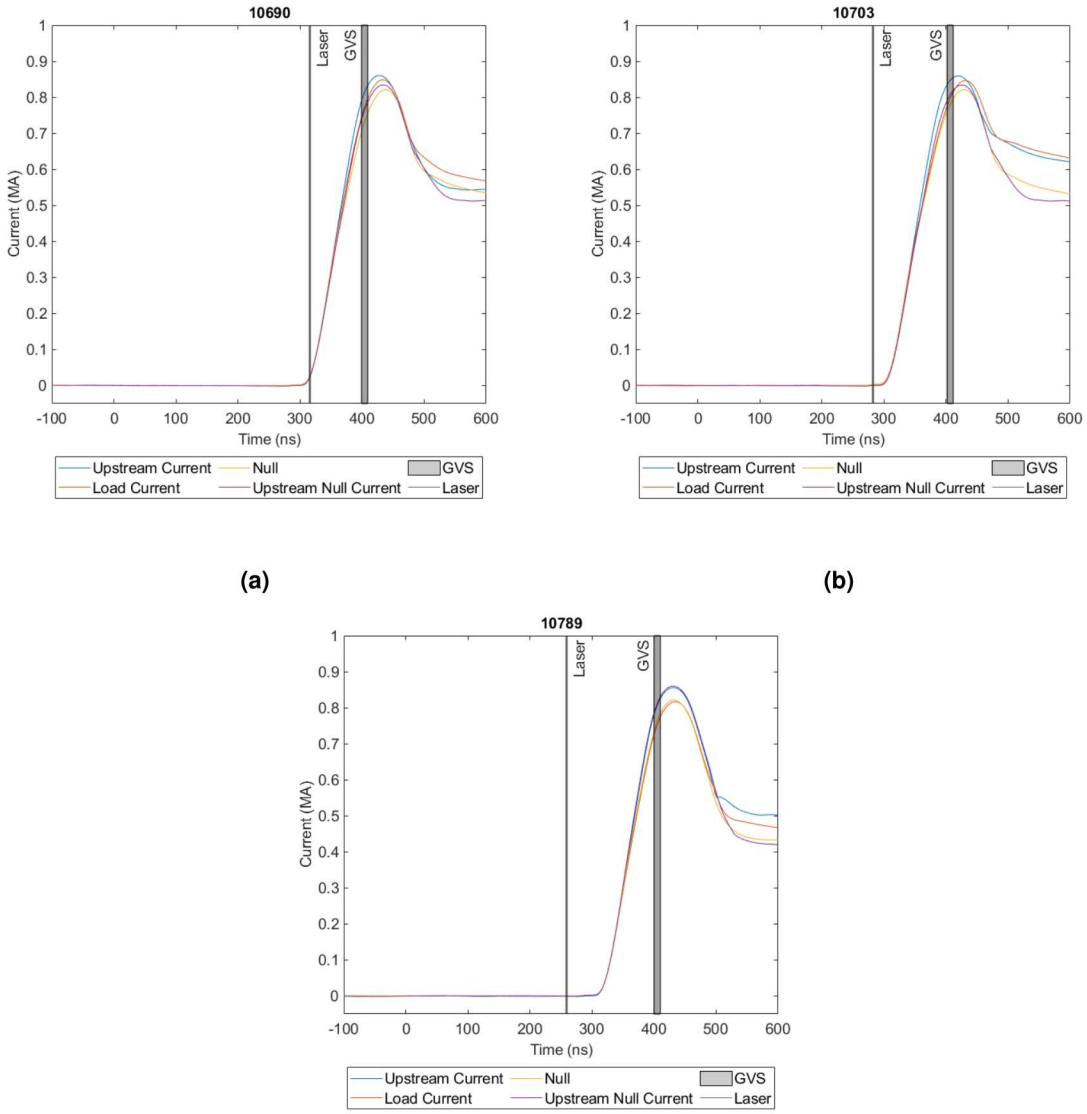

Figure 3-15 Current traces of three different NaCl dopant shots. (a) Laser: 111 ns before peak current. (b) Laser: 135 ns before peak current. (c) 175 ns before peak current. Shot 10690 had typical current traces, where the load current showed similar deviations from the upstream current as the null. Shot 10703 shows slightly earlier and more significant deviation from the upstream current, and shot 10695 showed significant loss compared to the null.

Shot 10703 was the first shot in a set of three NaCl dopant shots, all with laser energies between (45-54 mJ). The laser was moved 0.1 mm between each shot to avoid ablating material repetitively in the same position. The post shot spectra however was taken at the same location as the shot. As a result it is difficult to compare relative intensities except for the trend in which the post shot spectral lines are brighter than the shot lines. The post shot image shows sodium plasma extends through the entire AK gap, additionally the lines are significantly broadened during the

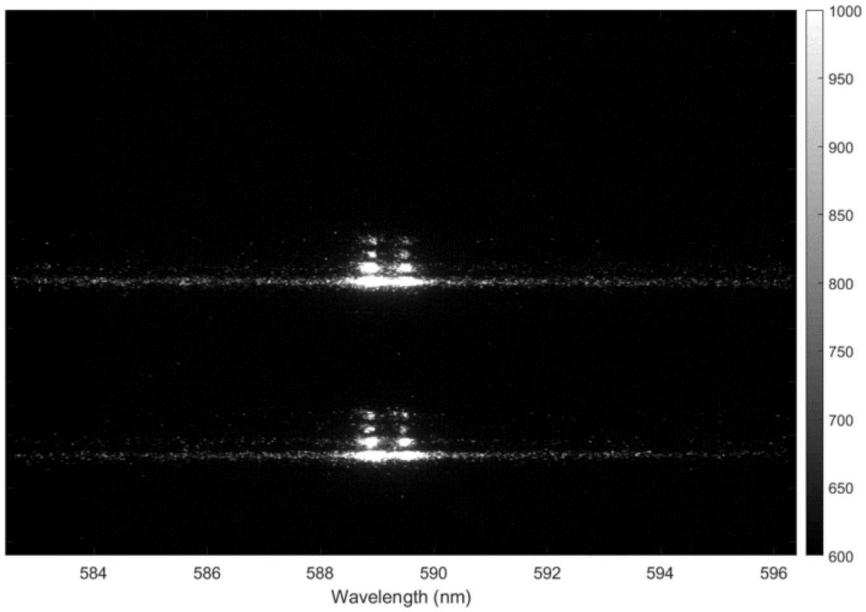

(a) Shot 10703, Post Shot

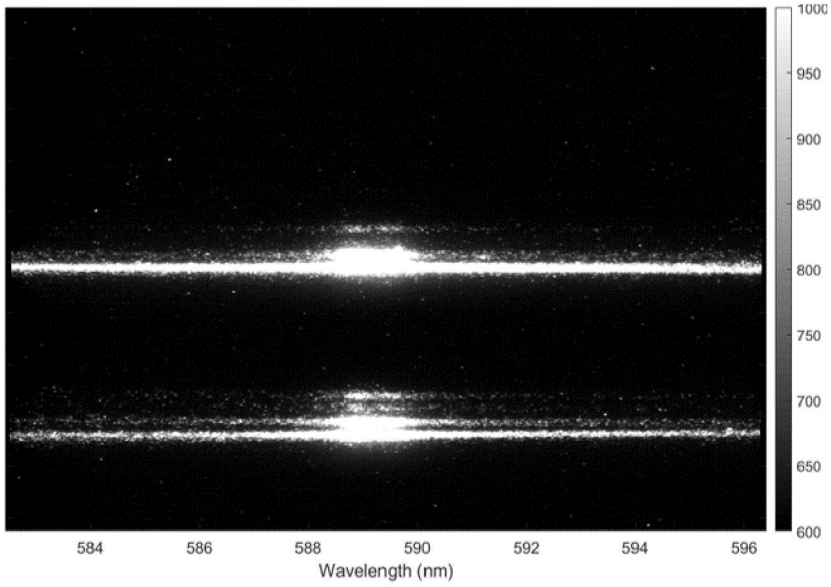

(b) Shot 10703, Shot, possible loss

Figure 3-16 Spectra from 10703. There appears to be a higher deviation from the upstream current b-dots compared to the null. See Figure 3-16 for current traces.

shot when compared to the post shot. As a result, it's possible that some current (10-20 kA) may be shunted through this channel that we are not able to measure with the B-dots. Fits to obtain density are in 3-17 and 3-18. Stark widths are from [4].

Off axis and on axis here refer to the fiber array column, and is not necessarily related to the densest part of the ablation plume. The solid targets like aluminum and copper can be repetitively fired until the fiber array is exactly aligned to the densest portion of the laser plasma. We were unable to use this method for the coated plugs without ablating most of the coating. Very small

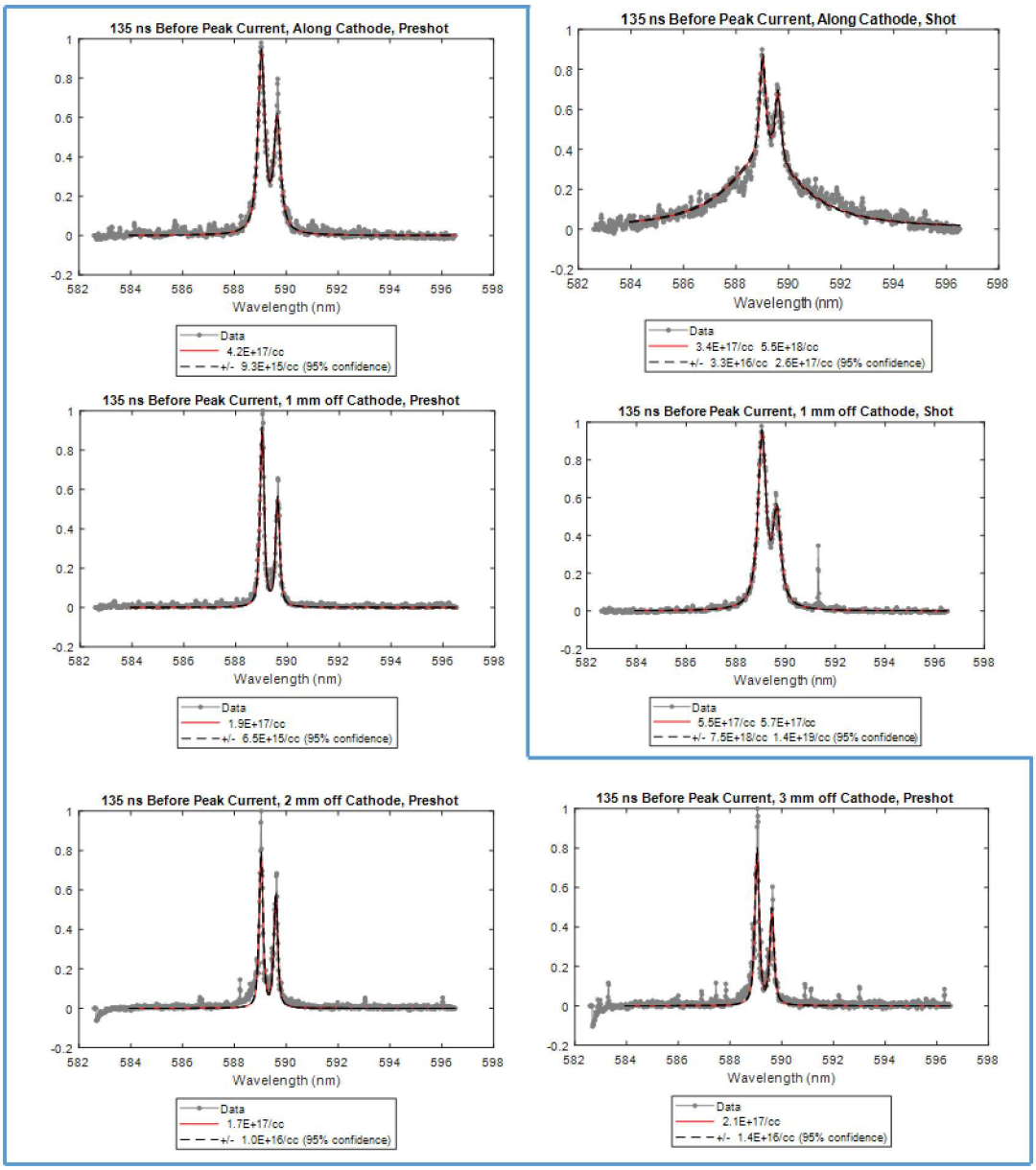

Figure 3-17 Shot 10703 line fits for on axis measurements. The blue box represents post shot spectra.

deviations in the laser alignment is enough to move the axis of the plume so that one column of the fiber array is no longer directly viewing the axis.

The electron density increases throughout the AK gap during the shot, with neutral Na I remaining in the gap. This is very different from what is seen in Figure 3-12. For example, 3 mm into the gap the average electron density increases by about 9.5e17/cc. This trend continues. By moving the laser even further back, as in shot 10695, Figure 3-16, the plasma across the gap becomes even more dense. This is shown in Figure 3-19, and significant loss current is measured. In this case it is difficult to compare the shot to the post shot. Typically, on shots in which

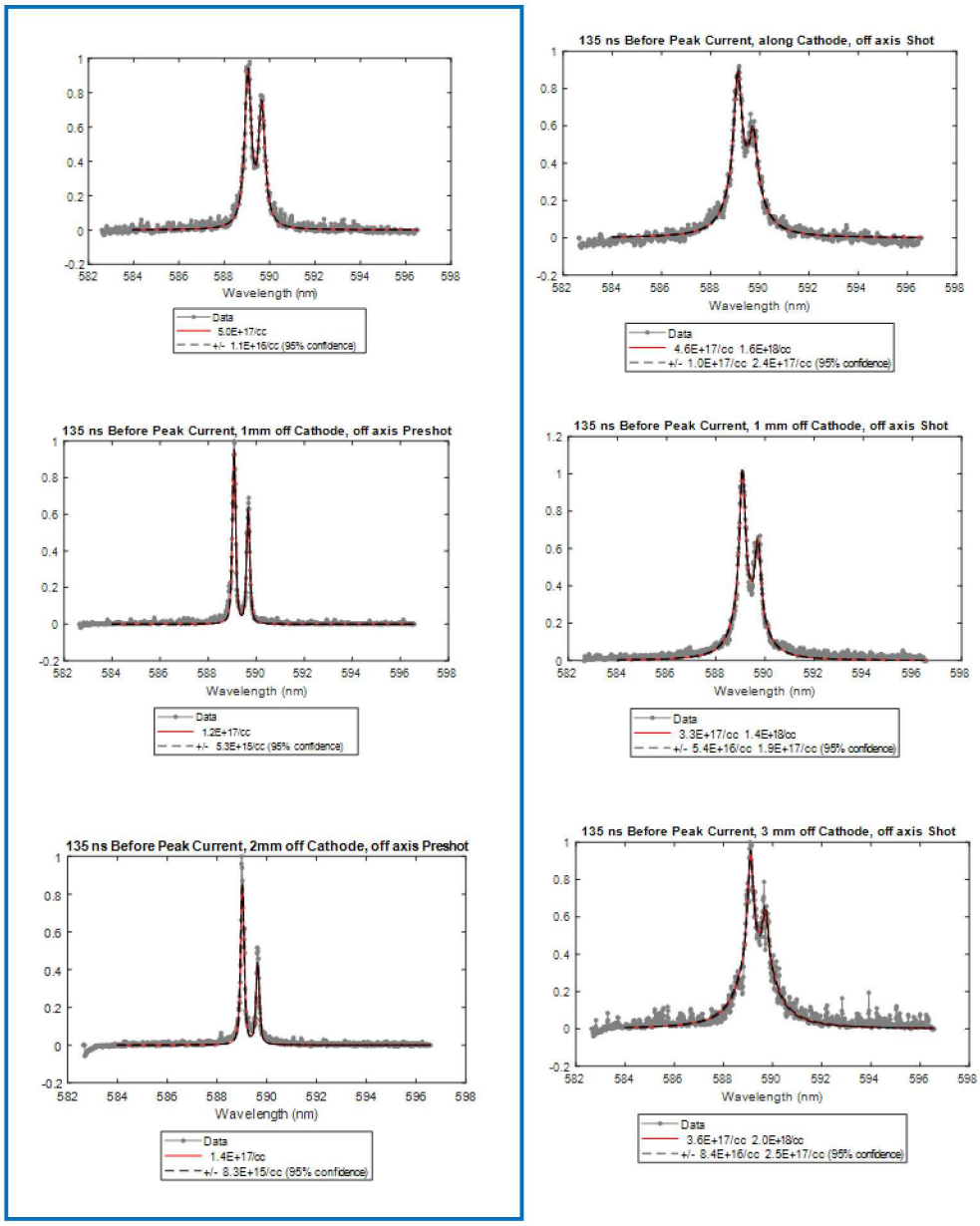

Figure 3-18 Shot 10703 line fits for off axis measurements. The blue box represents post shot spectra.

significant, measurable, current loss was detected, the dopant plug and laser focusing lens became coated with material and spectral measurements of the dopant lines were very weak as a result.

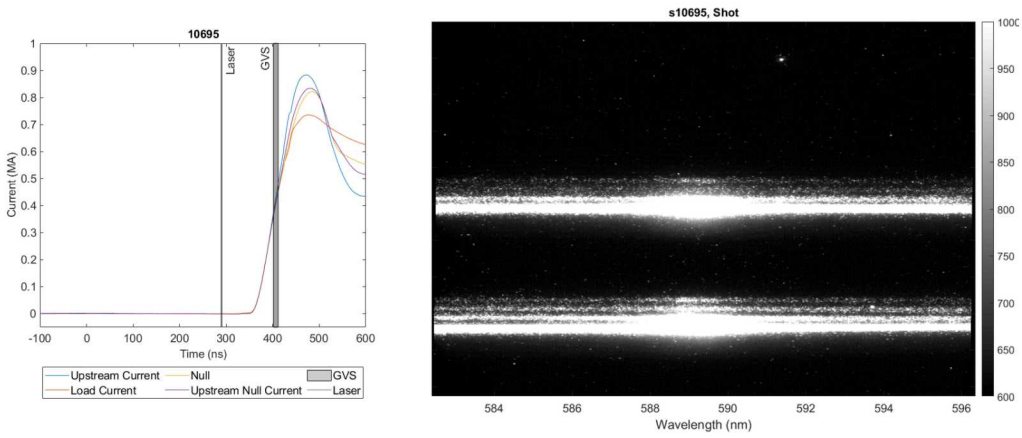

Figure 3-19 Spectra from 10695. Significant current loss was measured. See Figure 3-16 for current traces.

3.5. Lithium

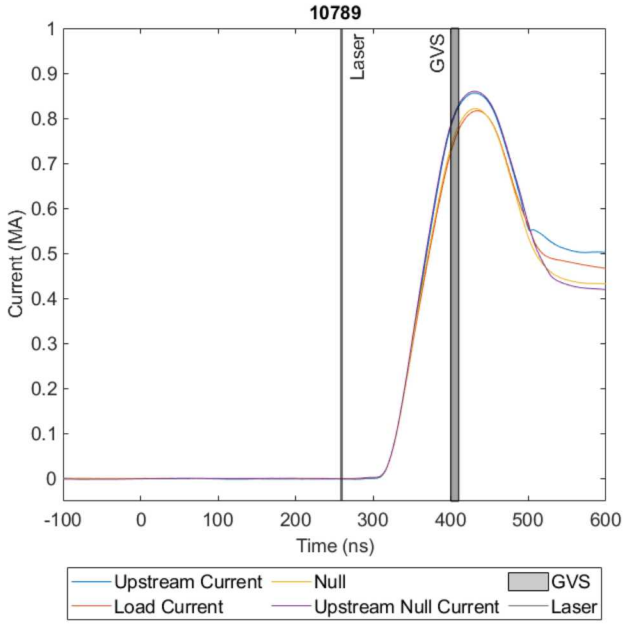

Figure 3-20 Current trace from Shot 10798. LiF coating on stainless steel plug. 42 mJ laser energy.

Similar to the NaCl coated stainless plug, 0.5 um LiF coatings were also used. Line emission from $1s^2 2p - 1s^2 3d$ at 610.4 nm and $1s^2 2s - 1s^2 2p$ at 670.8 nm were measured. These lines are of interest for B-field and E-field measurements on Z. The $1s^2 2p - 1s^2 3d$ line is particularly sensitive to E-fields [8], while $1s^2 2s - 1s^2 2p$ is in the strong B-field regime for the expected fields on Z. The gap was increased to 6.2 mm for many of the Li I measurements in order to

collect spectra earlier in the current pulse to try to obtain E-field estimates.

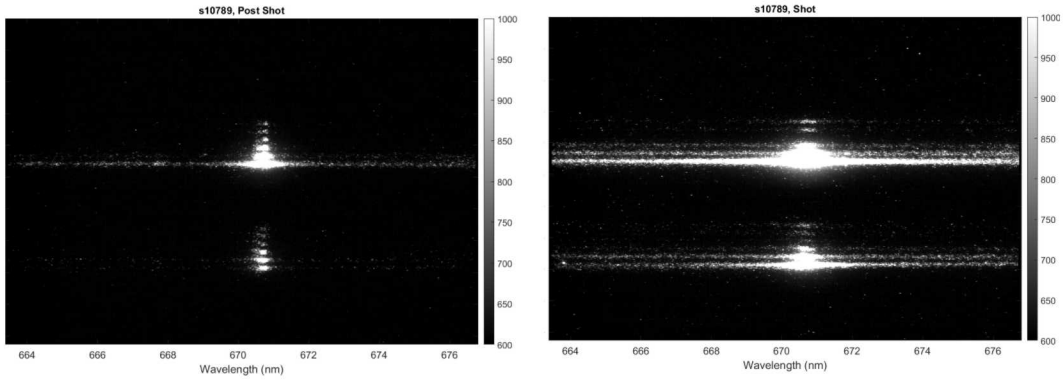

Figure 3-21 Spectra from 10789. 42 mJ Laser energy, 196 ns before peak current, 6.2 mm gap.

In Figure 3-21 we measure emission across a 6.2 mm gap without any evidence of gap shorting due to the ablation plasma, as shown in Figure 3-20, potentially do the the 2 mm increase in gap size. Analysis of these spectra are still progress. The fits shown in Figure 3-22 represent only Stark and instrument broadening. Further processing is needed to more accurately fit the line shapes. For example at 5.5 mm from the cathode (within 1 mm of the anode), the line shape appears "flat" at the peak, which may be an result of a magnetic field.

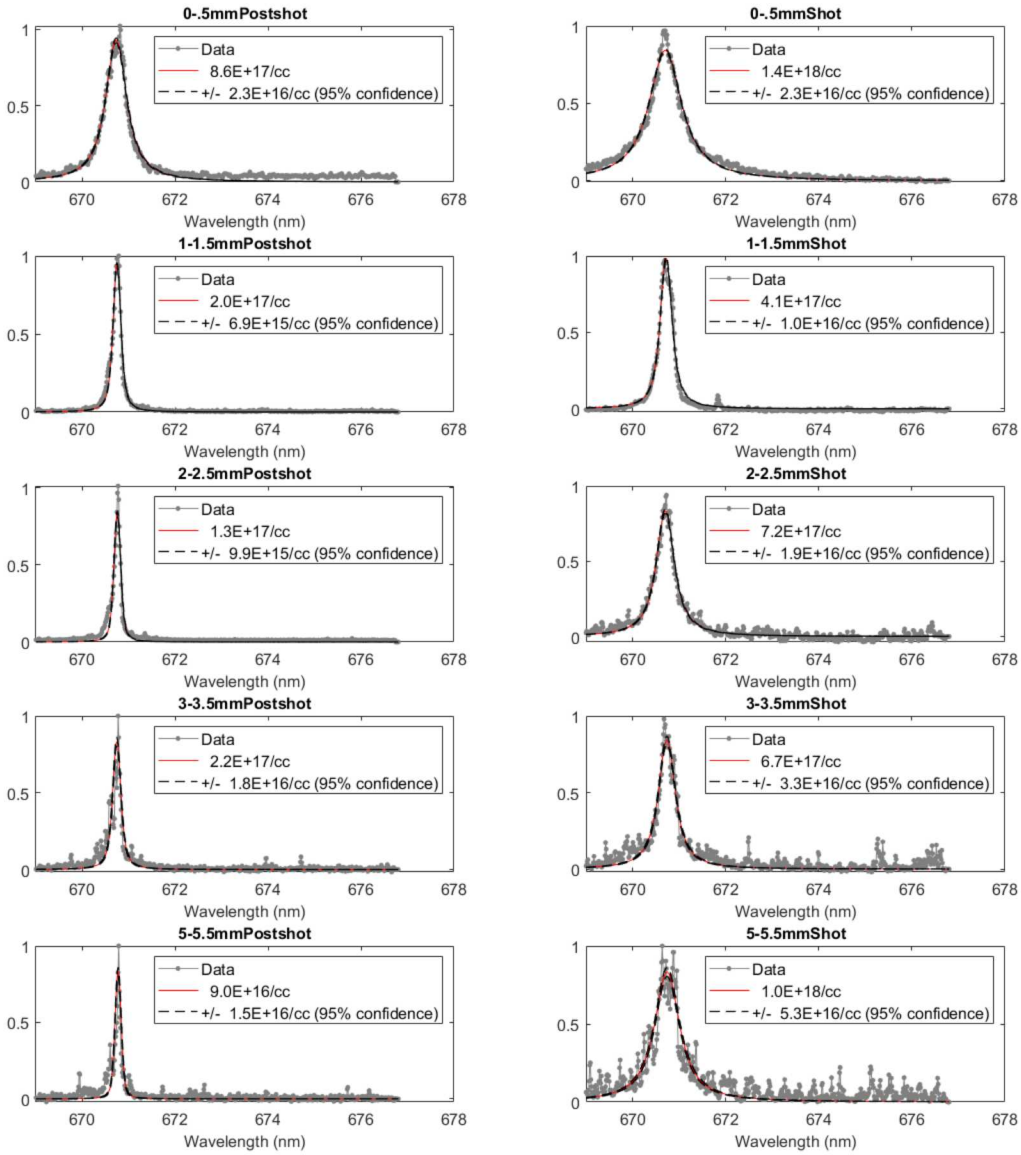

Figure 3-22 On axis fits of the Li I $1s^2 2s - 1s^2 2p$ transition, assuming only density and instrument broadening.

4. CONCLUSION

We have demonstrated that injecting a high density laser ablation plasma into the AK gap of a MITL does not appreciably affect power flow within some parameters. The primary parameter that appears to affect current delivery to the load is the time the ablation plasma forms. For a 4.5 ns gap, forming the ablation plasma earlier than 150 ns prior to peak current results in greater

plasma expansion through the gap, at higher densities, and increases the risk of current loss through the ablation plasma channel.

In order to prevent current loss we suggest timing the laser plasma to occur within 150 ns of peak current. While this can result in highly Stark dominated line shapes which can obscure small line shifts and splits due to fields, off axis measurements from the ablation plume can provide less dense plasma. A summary of shots is shown in Figure 4-1. In Figure 4-1 the peak load current is plotted for all shots that have an injected laser plasma and in which the vacuum insulator did not flash. The dopant material atomic weight does not seem to correlate with when the AK gap shorts, suggesting that other materials not measured are responsible for the gap shorting, such as hydrogen. Light lab measurements have shown hydrogen is always produced when ablating these materials.

Analysis of uncertainty, density changes, and potential field measurements are still in progress. However measurable differences in density and temperature in the ablation plasma are shown in this report for several shots and materials as a result of the Mykonos power pulse. It is still unclear hether this is due to MITL physics or current being shunted through the introduced plasma channel. The shunted current must be within the margin of error of the B-dots, which we currently expect to be a around less than 30 kA. For comparison [5] measured a 0.8 eV increase due to about 200 kA in the ablation plasma. Simulations may also provide insight into whether less than 30 kA of current can create the eV range temperature increases we measure, and 10^{17}/cc range density increases we measure during the pulse.

Now that we have determined the parameters with which we can create an ablation plasma with no noticeable effect on current delivery, we intend to bring this diagnostic to the Z-Machine. We expect this diagnostic can be more reliably used to diagnose electric and magnetic field strengths on Z than our current methods using passive dopants. We also expect the much higher electric and magnetic fields on Z should more appreciably affect these Stark dominated line shapes.

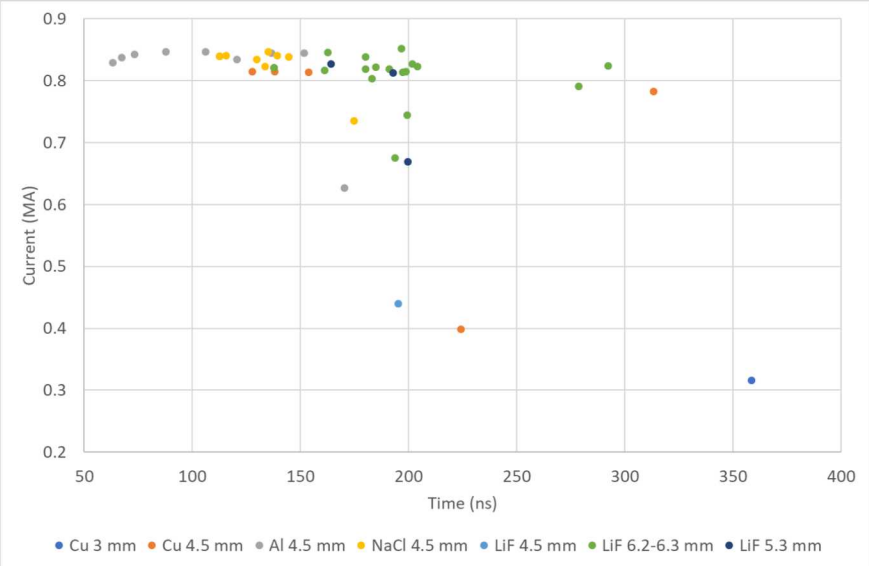

Figure 4-1 Peak current is plotted as a function of the difference between the time the laser hits the ablation target and peak current.

REFERENCES

[1] B. T. Hutsel, B. S. Stoltzfus, E. W. Breden, W. Fowler, P. A. Jones, D. Justus, F. W. Long, D. J. Lucero, K. A. MacRunnels, M. G. Mazarakis, *et al.*, "Millimeter-gap magnetically insulated transmission line power flow experiments," in *2015 IEEE Pulsed Power Conference (PPC)*, pp. 1–5, IEEE, 2015.

[2] T. Wagoner, W. Stygar, H. Ives, T. Gilliland, R. Spielman, M. Johnson, P. Reynolds, J. Moore, R. Mourning, D. Fehl, *et al.*, "Differential-output b-dot and d-dot monitors for current and voltage measurements on a 20-ma, 3-mv pulsed-power accelerator," *Physical Review Special Topics-Accelerators and Beams*, vol. 11, no. 10, p. 100401, 2008.

[3] "Prism computation sciences inc.," *PrismSPECT*, 1998.

[4] S. Sahal-Bréchot, M. Dimitrijević, and M. N., "Stark-b database, http://stark-b.obspm.fr,"

[5] E. Dutra, J. Koch, R. Presura, P. Wiewior, and A. Covington, "Electron temperature and electron number density measurements in laser ablation z-pinch experiments of al2o3," *Physics of Plasmas*, vol. 26, no. 8, p. 083506, 2019.

[6] S. Tessarin, D. Mikitchuk, R. Doron, E. Stambulchik, E. Kroupp, Y. Maron, D. Hammer, V. Jacobs, J. Seely, B. Oliver, *et al.*, "Beyond zeeman spectroscopy: Magnetic-field diagnostics with stark-dominated line shapes," *Physics of Plasmas*, vol. 18, no. 9, p. 093301, 2011.

[7] M. R. Gomez, S. B. Hansen, K. J. Peterson, D. Bliss, A. Carlson, D. Lamppa, D. Schroen, and G. Rochau, "Magnetic field measurements via visible spectroscopy on the z machine," *Review of Scientific Instruments*, vol. 85, no. 11, p. 11E609, 2014.

[8] J. Bailey, A. Filuk, A. Carlson, D. Johnson, P. Lake, E. McGuire, T. Mehlhorn, T. Pointon, T. Renk, W. Stygar, *et al.*, "Atomic emission spectroscopy in high electric fields," in *AIP Conference Proceedings*, vol. 381, pp. 245–258, American Institute of Physics, 1996.

APPENDIX A. TABLE OF ALL ACTIVE DOPANT SHOTS ON MYKONOS

Shot Number	Current (MA)	Gap	Dopant	Laser Energy (mJ)	Notes
s10590	0.500	3 mm	Cu		50 kV Calibration Shot
s10593	0.804	3 mm	Cu		Null
s10595	0.316	3 mm	Cu	112	
s10637	0.821	4.5 mm	Cu		Null Shot
s10638	0.782	4.5 mm	Cu	15	
s10641	0.815	4.5 mm	Cu	45	
s10642	0.813	4.5 mm	Cu	61	
s10643		4.5 mm	Cu		Null, insulator flash
s10645	0.815	4.5 mm	Cu	30	
s10646	0.813	4.5 mm	Cu		Null
s10648	0.821	4.5 mm	Cu	51	
s10650	0.399	4.5 mm	Cu	51	
s10654	0.829	4.5 mm	Al	45	
s10656	0.649	4.5 mm	Al	45	
s10661	0.838	4.5 mm	Al	45	
s10663	0.842	4.5 mm	Al	45	
unrecorded		4.5 mm	Al	45	Scopes were not set to record
s10667	0.847	4.5 mm	Al	45	
s10669	0.847	4.5 mm	Al	45	
s10671	0.835	4.5 mm	Al	45	
s10673				45	Insulator Flash
s10678	0.845	4.5 mm	Al	45	
s10680	0.845	4.5 mm	Al	45	
s10682	0.841	4.5 mm	Al	45	
s10684	0.627	4.5 mm	Al	45	
s10687	0.840	4.5 mm	NaCl	45	
s10690	0.840	4.5 mm	NaCl	45	
s10692	0.840	4.5 mm	NaCl	45	
s10695	0.735	4.5 mm	NaCl	45	
s10697	0.835	4.5 mm	NaCl	45	
s10699	0.823	4.5 mm	NaCl	45	
s10703	0.846	4.5 mm	NaCl	45	
s10705	0.839	4.5 mm	NaCl	57	
s10707	0.840	4.5 mm	NaCl	52	
s10711	0.440	4.5 mm	LiF	45	
s10714	0.846	6.3 mm	LiF	52	
s10717	0.839	6.3 mm	LiF	52	
s10720	0.852	6.3 mm	LiF	52	
s10722	0.853	6.3 mm	LiF		Null
s10724		6.3 mm	LiF	43	Insulator Flash

s10727	0.675	6.3 mm	LiF	43	
s10730	0.814	6.3 mm	LiF	40	
s10732	0.823	6.3 mm	LiF	40	
s10733	0.827	6.3 mm	LiF	40	
s10735	0.824	6.3 mm	LiF		Null
s10736	0.824	6.3 mm	LiF	40	
s10738	0.791	6.3 mm	LiF	40	
s10740	0.745	6.3 mm	LiF	40	
s10742	0.824	5.3 mm	LiF		Null
s10773	0.827	5.3 mm	LiF	40	
s10775	0.813	5.3 mm	LiF	40	
s10777	0.669	5.3 mm	LiF	40	
s10780	0.803	6.2 mm	LiF	42	
s10783	0.819	6.2 mm	LiF	42	
s10786	0.822	6.2 mm	LiF	42	
s10789	0.817	6.2 mm	LiF	42	
s10791	0.822	6.2 mm	LiF		Null
s10793	0.819	6.2 mm	LiF	42	
s10795	0.815	6.2 mm	LiF	42	
s10797	0.821	6.2 mm	LiF	42	

DISTRIBUTION

Email—Internal (encrypt for OUO)

Name	Org.	Sandia Email Address
Technical Library	01177	libref@sandia.gov

Sandia National Laboratories is a multimission laboratory managed and operated by National Technology & Engineering Solutions of Sandia LLC, a wholly owned subsidiary of Honeywell International Inc., for the U.S. Department of Energy's National Nuclear Security Administration under contract DE-NA0003525.